HHS Public Access

Author manuscript

*Biochemistry*. Author manuscript; available in PMC 2016 February 25.

Published in final edited form as:

*Biochemistry*. 2015 April 21; 54(15): 2539–2549. doi:10.1021/acs.biochem.5b00207.

# ABHD4 regulates multiple classes of *N*-acyl phospholipids in the mammalian central nervous system

**Hyeon-Cheol Lee**[1,2,*], **Gabriel M. Simon**[1,2], and **Benjamin F. Cravatt**[1,*]

[1]The Skaggs Institute for Chemical Biology and Department of Chemical Physiology, The Scripps Research Institute, 10550 N. Torrey Pines Road, La Jolla, CA 92037, USA

## Abstract

*N*-acyl phospholipids are atypical components of cell membranes that bear three acyl chains and serve as potential biosynthetic precursors for lipid mediators such as endocannabinoids. Biochemical studies have implicated ABHD4 as a brain *N*-acyl phosphatidylethanolamine (NAPE) lipase, but *in vivo* evidence for this functional assignment is lacking. Here, we describe ABHD4$^{-/-}$ mice and their characterization using untargeted lipidomics to discover that ABHD4 regulates multiple classes of brain *N*-acyl phospholipids. In addition to showing reductions in brain glycerophospho-NAEs (GP-NAEs) and plasmalogen-based lyso-NAPEs (lyso-pNAPEs), ABHD4$^{-/-}$ mice exhibited decreases in a distinct set of brain lipids that were structurally characterized as *N*-acyl lysophosphatidylserines (lyso-NAPSs). Biochemical assays confirmed that NAPS lipids are direct substrates of ABHD4. These findings, taken together, designate ABHD4 as a principal regulator of *N*-acyl phospholipid metabolism in the mammalian nervous system.

Lipids serve several fundamental roles in biology, including providing the chemical matter for cell membrane structures and acting as signaling molecules that bind to protein receptors to regulate diverse physiological processes.[1] Phospholipids are a large class of lipids that contain a glycerol backbone esterified with two fatty acyl chains and conjugated through its third hydroxyl to a phosphate head group. The phosphate in most phospholipids is further modified with a polar substituent, such as those found in phosphatidylcholine (choline), phosphatidylethanolamine (ethanolamine), and phosphatidylserine (serine). *N*-acyl phospholipids, however, represent an unusual class of phospholipids that contain head groups modified with fatty acids.[2, 3] Two major types of *N*-acyl phospholipids have been discovered in mammals – *N*-acyl phosphatidylethanolamines (NAPEs) and *N*-acyl phosphatidylserines (NAPSs) (Figure 1). The presence of a third fatty acid group grants *N*-acyl phospholipids with substantially altered physicochemical properties compared to other classes of phospholipids. Although the initial structural characterization of *N*-acyl phospholipids as endogenous constituents of mammalian tissues occurred several decades

*Correspondence: hclee@scripps.edu (H.L.) or cravatt@scripps.edu (B.F.C.).

[2]These authors contributed equally to this work

**Associated Content**

**Supporting Information**.

Supporting tables and figures. This material is available free of charge via the Internet at http://pubs.acs.org.

ago,[4, 5] we still today have only a limited understanding of the biological functions and routes for enzymatic metabolism of this class of lipids.

NAPEs are considered rare phospholipids and, under physiological conditions, account for ~0.01% of total phospholipids of animal membranes.[2, 3] However, NAPEs can accumulate under conditions of injury or stress.[2, 3] Owing to the presence of a third acyl chain, *N*-acyl phospholipids impart stabilizing properties on cell membranes,[6] as well as displaying fusogenic potential.[7] Beyond these structural roles, some NAPEs may function as signaling molecules, as N-palmitoyl phosphatidylethanolamine has been shown to regulate food intake in mice[8] and inflammatory responses.[9] Arguably, however, NAPEs are most well recognized as precursors to the N-acyl ethanolamine (NAE) class of signaling lipids, which includes the endocannabinoid anandamide (C20:4 NAE).[10] The conversion of NAPEs to NAEs can occur through one of multiple enzymatic routes, including direct phospholipase D-mediated catalysis by an NAPE-PLD[11–14] and multi-step pathways that proceed through phospholipase $A_{1/2}$[15–17] and C[18, 19] enzymes. Plasmalogen-based NAPEs (pNAPEs) are a major subclass of NAPEs and can also be catabolized by NAPE-PLD, as well as the combined action of a pNAPE lipase and lyso-pNAPE phospholipase D.[14] The biosynthesis of NAPEs appears to involve both calcium-dependent and –independent transacylase enzymes that transfer the fatty acid groups from phospholipids onto the amine of phosphatidylethanolamine.[20–24] While the calcium-dependent transacylase remains molecularly uncharacterized, HRAS-like suppressor family proteins have been shown to function as calcium-independent transacylases that produce NAPEs.[25–32] The NAPS class of N-acyl phospholipids, which has been isolated from human brain, animal tissues and cells, as well as yeast[33, 34], is less well-characterized in terms of its biological functions and metabolism.

NAPE-PLD$^{-/-}$ mice exhibit massive increases in brain NAPE and lyso-NAPE content (~10-fold), but only modest reductions in major NAEs (~two-fold or less), including C16:0, C18:0, C18:1, and C20:4 NAEs.[13, 14] These findings pointed to the existence of additional pathways for metabolizing NAPEs. One candidate pathway is mediated by $PLA_{1/2}$ enzymes to yield lysoNAPE and glycerophospho (GP)-NAE intermediates, which would then be metabolized further to NAEs.[10] The serine hydrolase ABHD4 has been identified as an NAPE and lyso-NAPE lipase with strong expression in brain.[17] The function of ABHD4 *in vivo*, however, remains unknown. In this manuscript, we describe the generation and characterization of ABHD4$^{-/-}$ mice. Lipidomic analysis of brain tissue from these animals uncovered significant reductions in not only glycerophospho-NAEs (GP-NAEs) and lyso-pNAPEs, but also lyso-NAPSs. Recombinant ABHD4 was found to hydrolyze NAPS. These data thus indicate that ABHD4 is a principal enzyme responsible for the hydrolytic metabolism of both the NAPE and NAPS classes of *N*-acyl phospholipids *in vivo*.

## EXPERIMENTAL PROCEDURES

### Materials

$d_4$-anandamide and $d_8$-anandamide were purchased from Cayman Chemicals. 1,2-dioleoyl-*sn*-glycero-3-phosphoethanolamine (PE), 1-oleoyl-2-hydroxy-*sn*-glycero-3-phosphoethanolamine (lysoPE), 1-*O*-1'-(*Z*)-octadecenyl-2-oleoyl-*sn*-glycero-3-

phosphoethanolamine (plasmenyl PE), 1-*O*-1'-(*Z*)-octadecenyl-2-hydroxy-*sn*-glycero-3-phosphoethanolamine (plasmenyl lysoPE), 1-stearoyl-2-oleoyl-*sn*-glycero-3-phosphoserine (PS), 1-stearoyl-2-hydroxy-*sn*-glycero-3-phosphoserine (lysoPS), 1-hexadecanoyl-L-serine, and 1-(5*Z*, 8*Z*, 11*Z*, 14*Z*–eicosatetraenoyl)-L-serine were purchased from Avanti Polar Lipids (Alabaster, AL). Heptadecenoic acid, pentadecenoyl chloride, palmitoyl chloride, heptadecenoyl chloride, nonadecenoyl chloride, and arachidonoyl chloride were purchased from NuCheck Prep (Elysian, MN). 1,2-dioleoyl-*sn*-glycero-3-phospho (*N*-nonadecenoyl) ethanolamine, 1,2-dioleoyl-*sn*-glycero-3-phospho (*N*-arachidonoyl) ethanolamine, 1-*O*-1'-(*Z*)-octadecenyl-2-oleoyl-*sn*-glycero-3-phospho (*N*-nonadecenoyl) ethanolamine, 1-oleoyl-2-hydroxy-*sn*-glycero-3-phospho (*N*-pentadecenoyl) ethanolamine, 1-oleoyl-2-hydroxy-*sn*-glycero-3-phospho (*N*-palmitoyl) ethanolamine, 1-oleoyl-2-hydroxy-*sn*-glycero-3-phospho (*N*-heptadecenoyl) ethanolamine, 1-*O*-1'-(*Z*)-octadecenyl-2-hydroxy-*sn*-glycero-3-phospho (*N*-heptadecenoyl) ethanolamine were synthesized as described.[17, 35] Briefly, acid chlorides were reacted with an excess of PE, plasmenyl PE, lysoPE, or plasmenyl lysoPE and allowed to react for 1 h in $CH_2Cl_2$ with a catalytic amount of triethylamine. *N*-acylated lipids were then purified by silica gel flash column chromatography or preparative TLC. 1,2-dihydroxy-*sn*-glycero-3-phospho (*N*-pentadecenoyl) ethanolamine was synthesized by base hydrolysis of 1-oleoyl-2-hydroxy-*sn*-glycero-3-phospho (*N*-pentadecenoyl) ethanolamine as described.[17, 35] The synthetic phospholipid standards were evaluated by LC-MS to assess purity and quantified by the Bartlett assay.[36] More detailed synthetic methods are described below.

## Generation of ABHD4$^{-/-}$ Mice

Construction of mice bearing a disruption in the *Abhd4* gene was achieved using a standard targeting strategy in CMTI-1 embryonic stem cells from the 129S6/SvEvTac strain. Genomic DNA corresponding to a region including exons 3 and 4 of *Abhd4* was amplified from a BAC clone isolated from the RPCI-22 library. Identification of neomycin-resistant ES cell clones bearing homologous recombination events was achieved via southern blot using a probe that hybridizes downstream of the targeting construct. Recombinant clones were injected into blastocysts from C57BL/6 mice and germline-transmission was determined by coat-color. Tail DNA from brown mice was subjected to southern-blotting using a probe that hybridizes upstream of the targeting construct, thereby confirming true homologous recombination. These mice were back-crossed into the C57BL/6 background for ten generations prior to biochemical and lipidomic analyses.

## Preparation of Mouse Tissue Proteomes

Mice were anesthetized with isoflurane and killed by decapitation. Brains were immediately removed and snap-frozen in liquid $N_2$. Frozen brains were dounce-homogenized on ice in PBS (pH 7.4) and centrifuged at 1,000 × g for 10 minutes to remove debris. The resulting supernatant was further centrifuged at 100,000 × g for 45 minutes to provide the soluble fraction in the supernatant and the membrane fraction as a pellet. The pellet was washed and resuspended in PBS by brief sonication. Protein concentrations were determined using the DC Protein Assay (Bio-Rad), and samples were stored at −80 °C until use.

### Gel-based ABPP Analysis

Brain soluble and membrane proteomes (50 μg in 50 μL of PBS) were prepared from 2-week-old ABHD4$^{+/+}$ and ABHD4$^{-/-}$ females and incubated with 1 μM FP-rhodamine for 30 min at 37 °C. After 30 minutes reactions were quenched with 4x SDS/PAGE loading buffer (reducing), separated by SDS/PAGE [10% (wt/vol) acrylamide] and visualized by in-gel fluorescence scanning (Hiatchi FMBio IIe, MiraBio). Rhodamine fluorescence is shown in gray scale.

### Mass Spectrometry (MS)-based Proteomics

Serine hydrolase enrichment was performed essentially as described.[37] Briefly, brain proteomes were adjusted to a final protein concentration of 2 mg/mL and treated with FP-biotin (500 μL total reaction volume, 10 μM final concentration) for 2 hours at room temperature. Excess probe was removed by protein precipitation using 4:1 (vol/vol) methanol:chloroform and proteins were then dissolved in 6 M urea in 25 mM ammonium bicarbonate. Proteins were reduced with 10 mM DTT, alkylated with 40 mM iodoacetamide, and diluted to a final concentration of 2 M urea with 25 mM ammonium bicarbonate. Biotinylated proteins were then enriched with avidin beads (SIGMA; #A9207) by incubation for 2 h at room temperature in 0.2% SDS in DPBS. The beads were washed three times with 1% SDS in DPBS, then three additional times in DPBS, then resuspended in 25 mM ammonium bicarbonate with 2 M urea. On-bead digestion with 2 μg trypsin (Promega; #V511A) was performed overnight at 37 °C in the presence of 1 mM $CaCl_2$. Tryptic digests were acidified with 5% (vol/vol) formic acid, and aliquots were frozen at −80 °C until use. Multidimensional liquid chromatography tandem mass spectrometry (MudPIT) analysis was performed as described previously[38] and peptides were eluted directly into a Velos Orbitrap mass spectrometer (Thermo Fisher) essentially as previously described.[37] See Table S1 for data complete list of serine hydrolases detected in these experiments.

### Cell Culture and Transfection

COS-7 cells were grown at 37 °C and 5% $CO_2$ to ~70% confluence in Dulbecco's modified Eagle's medium containing 10% fetal calf serum in 10 cm dishes and transfected with 5 μg of plasmid DNA (or empty vector control) using polyethyleneimine (Polysciences, Warrington, PA, USA). After 24 h, the cells were washed twice with PBS, scraped, resuspended in PBS, and sonicated to lyse. The lysates were spun at 100,000 x g for 45 min to isolate the cytosolic fraction.

### Plasmids

Full-length mouse *Abhd4* was amplified by PCR from mouse brain cDNA with primers Abhd4 forward (5′-TGGTGGAATTCGCCACCATGGGCTGGCTCAGCTCGAC-3′) and reverse (5′-ACCTATCTAGAGTCAACTGAGTTGCAGATCT-3′) and was cloned into the pcDNA3.1/Myc-His vector with a C-terminal Myc-His tag using EcoRI and XbaI sites.

### *In vitro* Enzyme Assays

Detection of (lyso)phospholipid hydrolysis was accomplished via mass-spectrometric detection of the release of oleic acid or lyso-NAPE from substrates. Enzyme assays were

performed in PBS in a total volume of 100 μl using 0.5 mg/ml protein. To avoid contaminating signals from endogenous lipids, soluble extracts of brain or cells were assayed. Reactions were incubated at 37 °C for 1 h with 100 μM substrate, 2 mM EDTA, with or without 0.1% Triton X-100. Reactions were stopped by the addition of 500 μl of MeOH and 1 nmol of heptadecenoic acid or 100 pmol of 1-oleoyl-2-hydroxy-*sn*-glycero-3-phospho (*N*-heptadecenoyl) ethanolamine was added as an internal standard. Lipids were extracted by the Bligh and Dyer method.[39] A portion of the extracted lipid was injected onto an Agilent 6520 series quadrupole-time-of-flight (Q-TOF) MS. Chromatography was performed on a 50 × 4.60 mm 5 μm Gemini C18 column (Phenomenex) coupled to a guard column (Gemini; C18; 4 × 3.0 mm; Phenomenex SecurityGuard cartridge). The LC method consisted of 0.1 ml/min of 100% buffer A [95:5 (vol/vol) $H_2O$:MeOH plus 0.1% (vol/vol) of 28% ammonium hydroxide] for 1.5 min, 0.5 ml/min linear gradient to 100% buffer B [60:35:5 (vol/vol) iPrOH:MeOH:$H_2O$ plus 0.1% (vol/vol) of 28% ammonium hydroxide] over 5 min, 0.5 ml/min 100% buffer B for 5.5 min, and equilibration with 0.5 ml/min 100% buffer A for 3 min (15 min total run time). MS analysis was performed in negative scanning mode with an electrospray ionization (ESI) source. The capillary voltage was 4.0 kV, the fragmentor voltage was 100 V, the drying gas temperature was 350 °C, the drying gas flow rate was 11 l/min, and the nebulizer pressure was 45 psi. Oleic acid release or lyso-NAPE release was quantified by measuring the area under the peak and comparing to the heptadecenoic acid or lyso-NAPE standard, respectively.

## Untargeted Metabolomics Analysis

Discovery metabolite profiling (DMP) was performed as described previously.[40] ABHD4$^{+/+}$ and ABHD4$^{-/-}$ mice from 2 to 4 months of age ($n$ = 4 per genotype) were anesthetized with isoflurane and killed by decapitation. Brains were harvested, laterally sectioned, and immediately submerged in liquid $N_2$. One frozen brain hemisphere per mouse was weighed and immediately Dounce-homogenized in 8 ml of 2:1:1 (vol/vol/vol) $CHCl_3$:MeOH:50 mM Tris pH8.0 with heptadecenoic acid and $d_8$-anandamide added as internal standards for negative- and positive-mode analysis, respectively. Homogenates were centrifuged for 10 min at 1,400 × g. The organic (lower) phase was transferred to a clean vial and dried under a stream of $N_2$. The metabolomes were resolubilized in 2:1 vol/vol $CHCl_3$:MeOH (120 μl), and 30 μl was injected onto an Agilent 6520 series quadrupole-time-of-flight (Q-TOF) MS. LC separation was achieved using the same solid and mobile phases described above for substrate assays. To assist in ion formation, 0.1% (vol/vol) of 28% ammonium hydroxide or 0.1% (vol/vol) formic acid was added to the buffers for negative or positive ionization mode, respectively. The LC method consisted of 0.1 ml/min 0% buffer B for 5 min, a 0.4 ml/min linear gradient over 40 min to 100% buffer B, 0.5 ml/min 100% buffer B for 10 min, and 0.4 ml/min equilibration with 0% buffer B for 5 min, for an overall run time of 60 min. MS analysis was performed with an ESI source in scanning mode from $m/z$ = 50–1,200. The capillary voltage was set to 4.0 kV, and the fragmentor voltage was set to 100 V. The drying gas temperature was 350 °C, the drying gas flow rate was 11 l/min, and the nebulizer pressure was 45 psi. Analysis of the LC-MS data were performed with the XCMS software,[41, 42] which identifies, matches, aligns, and integrates chromatographic peaks and identifies $m/z$ values that are significantly altered in control vs. experimental datasets. XCMS results from two independently performed experiments were compared and filtered

for *m*/*z* values that appeared in both datasets with greater than three-fold change between genotypes, greater than 10,000 average peak-integration area, LC elution time during the linear gradient, and $P < 0.01$. Obvious isotopic peaks were manually excluded. Results are presented as the ratio of the average peak area measured in the ABHD4$^{+/+}$ vs. ABHD4$^{-/-}$ brain metabolomes. Putative assignments were confirmed by coelution with synthetic standards and/or fragmentation analysis as described below. Relative abundance of known lipid species was determined by manually extracting the mass corresponding to the $[M - H]^-$ or $[M + H]^+$ parent ion (in negative- or positive-ionization mode, respectively), integrating the area under the peak and normalizing this value for the tissue weight and internal standard area peak. Statistical significance was determined by unpaired, two-tailed Welch's t test.

### Tandem MS Fragmentation Experiments

MS/MS analysis was performed on an Agilent 6520 series quadrupole-time-of-flight (Q-TOF) instrument, using the same LC separation and buffers as described above for untargeted metabolomics. MS and MS/MS data collection, both in scanning mode from *m*/*z* = 50–1200 and a rate of 1.0 spectra/s, was performed with an electrospray ionization (ESI) source. The capillary voltage was set to 4.0 kV and the fragmentor voltage was set to 100 V. The drying gas temperature was 350°C, the drying gas flow rate was 11 l/min, and the nebulizer pressure was 45 psi. The collision energy was set to 20 V for lyso-NAPS and 15 V for NAS.

### Targeted Metabolite Measurements

NAPEs, pNAPEs, lyso-NAPEs, lyso-pNAPEs, GP-NAEs, NAEs, NAPSs, and lyso-NAPSs in brains from ABHD4$^{+/+}$ and ABHD4$^{-/-}$ mice 2 months of age were measured by multiple reaction monitoring (MRM) methods. Brains were harvested and the metabolomes were extracted as described above. 30 μl of lipid extract was injected onto an Agilent 6460 series triple-quadrupole MS connected to an Agilent 1290 Infinity HPLC system. LC separation was achieved using the solid and mobile phases described above for untargeted metabolomics and the following method: 0.1 ml/min 0% buffer B for 5 min, a 0.4 ml/min linear gradient over 15 min to 100% buffer B, 0.5 ml/min 100% buffer B for 8 min, and 0.4 ml/min equilibration with 0% buffer B for 5 min (33 min total run time per sample). For measurements in negative mode, 0.1% (vol/vol) of 28% ammonium hydroxide was added to the buffers. For measurements in positive mode, 0.1% (vol/vol) of formic acid or 10 mM ammonium formate was added to the buffers. For NAPEs and pNAPEs, MRM transition from $[M - H]^-$ to the fragment ion $[R_2COO]^-$ with collision energy 45 V was used. Absolute abundance of NAPEs and pNAPEs were estimated by comparison to the *N*-19:1 NAPE (1,2-dioleoyl-*sn*-glycero-3-phospho (*N*-nonadecenoyl) ethanolamine) standard. For pNAPEs, the extraction and ionization efficiencies of *N*-19:1 pNAPE (1-*O*-1'-(*Z*)-octadecenyl-2-oleoyl-*sn*-glycero-3-phospho (*N*-nonadecenoyl) ethanolamine) were compared to those of the *N*-19:1 NAPE standard, and the levels of pNAPEs were corrected accordingly. For lyso-NAPEs, MRM transition from $[M - H]^-$ to the fragment ion $[R_1COO]^-$ or $[R_2COO]^-$ with collision energy 35 V was used. Absolute abundance of lyso-NAPEs was estimated by comparison to the *N*-17:1 lyso-NAPE (1-oleoyl-2-hydroxy-*sn*-glycero-3-phospho (*N*-heptadecenoyl) ethanolamine) standard. For GP-NAEs, MRM transition from $[M - H]^-$ to the fragment ion [deprotonated glycerophosphate]$^-$ at *m*/*z* 171

with collision energy 24 V was used. Absolute abundance of GP-NAEs was estimated by comparison to the *N*-15:1 GP-NAE (1,2-dihydroxy-*sn*-glycero-3-phospho (*N*-pentadecenoyl) ethanolamine) standard. Extraction efficiencies for *N*-15:1, *N*-16:0, *N*-18:0, and *N*-18:1 GP-NAEs under these conditions were 2.3, 10.5, 36.6, and 22.0%, respectively, and endogenous GP-NAE levels were corrected accordingly. For certain GP-NAE measurements (Figure S1C), 1% formic acid was used for the aqueous phase of the lipid extraction, rather than Tris pH 8. Under these conditions, extraction efficiencies for *N*-15:1, *N*-16:0, *N*-18:0, and *N*-18:1 GP-NAEs were 62.2, 78.2, 83.4, and 78.9%, respectively, and measurements of endogenous species were corrected accordingly. For NAPSs, MRM transition from $[M - H]^-$ to the fragment ion [phosphatidic acid]$^-$(loss of *N*-acyl serine) with collision energy 35 V was used. Absolute abundance of NAPSs was estimated by comparison to the *N*-17:1 NAPS (1-stearoyl-2-oleoyl-*sn*-glycero-3-phospho (*N*-heptadecenoyl) serine) standard. For lyso-NAPSs, MRM transition from $[M - H]^-$ to the fragment ion [lyso phosphatidic acid]$^-$ (loss of *N*-acyl serine) with collision energy 20 V was used. Abundance of lyso-NAPSs was compared to the internal *N*-17:1 lyso-NAPS (1-stearoyl-2-hydroxy-*sn*-glycero-3-phospho (*N*-heptadecenoyl) serine) standard, however the amount of synthesized *N*-17:1 lyso-NAPS standard was too low to permit absolute quantitation so the values are reported as arbitrary units. For NASs, MRM transition from $[M - H]^-$ to the fragment ion $[C_2H_4NO_2]^-$ with collision energy 15 V was used. Absolute abundance of NASs was estimated by comparison to the *N*-17:1 NAS (1-heptadecenoyl-L-serine) standard. For NAEs, formic acid was included in the mobile phase and MRM transition from $[M + H]^+$ to *m*/*z* 62 (ethanolamine fragment) with collision energy 11 V was used, except for the $d_4$-anandamide standard which monitored the transition from $[M + H]^+$ to *m*/*z* 66 ($d_4$ ethanolamine fragment). NAEs were quantified by comparison to the $d_4$-anandamide standard. For lyso pNAPEs ammonium formate was added to the buffers and MRM transition from $[M + H]^+$ to $[CH_2CH_2NHCOR_N]^+$ with collision energy 15 V was used. Absolute abundance of lyso pNAPEs was estimated by comparison to the *N*-17:1 lyso-NAPE standard. The extraction and ionization efficiencies of *N*-17:1 lyso pNAPE (1-*O*-1'-(*Z*)-octadecenyl-2-hydroxy-*sn*-glycero-3-phospho (*N*-heptadecenoyl) ethanolamine) were compared to those of the *N*-17:1 lyso-NAPE standard, and the levels of lyso pNAPEs were corrected accordingly. MS analyses were performed by multiple reaction monitoring (MRM) with an ESI source. The capillary voltage was set to 3.5 kV, and the fragmentor voltage was set to 100 V. The drying gas temperature was 350 °C, the drying gas flow rate was 9 l/min, and the nebulizer pressure was 45 psi. The dwell time for each lipid was set to 100 ms.

## Chemical Syntheses of Lipid Standards and Substrates

**Synthesis of 1-stearoyl-2-hydroxy-sn-glycero-3-phospho (N-palmitoyl) serine —**A solution of 1-stearoyl-2-hydroxy-*sn*-glycero-3-phosphoserine (3.0 mg, 5.7 μmol, 1.0 equiv.) in $CH_2Cl_2$ (1 mL) and triethylamine (12.5 μL) was treated with palmitoyl chloride (1.4 mg, 5.1 μmol, 0.9 equiv.), and the reaction mixture was stirred for 1 h at ambient temperature. The reaction was concentrated under a stream of $N_2$, and the remaining residue was purified by preparative TLC ($CHCl_3$:MeOH:$NH_4OH$:$H_2O$ = 65:35:5:1) providing the title compound. HRMS (ESI-TOF-) *m*/*z* calc'd for $C_{40}H_{77}NO_{10}P$ $[M - H]^-$: 762.5290, found 762.5297. 1-stearoyl-2-oleoyl-*sn*-glycero-3-phospho (*N*-palmitoyl) serine (HRMS (ESI-TOF-) *m*/*z* calc'd for $C_{58}H_{109}NO_{11}P$ $[M - H]^-$: 1026.7743, found 1026.7746.), 1-

stearoyl-2-oleoyl-*sn*-glycero-3-phospho (*N*-heptadecenoyl) serine (HRMS (ESI-TOF-) *m*/*z* calc'd for $C_{59}H_{109}NO_{11}P$ $[M - H]^-$: 1038.7743, found 1038.7743.), and 1-stearoyl-2-hydroxy-*sn*-glycero-3-phospho (*N*-heptadecenoyl) serine (HRMS (ESI-TOF-) *m*/*z* calc'd for $C_{41}H_{77}NO_{10}P$ $[M - H]^-$: 774.5290, found 774.5286.) were synthesized from their corresponding PS and lyso-PS analogs and characterized in the same manner.

**Synthesis of 1-heptadecenoyl-L-serine (N-17:1 NAS)—**L-Serine (27.4 mg, 0.26 mmol, 1.5 equiv.) was dissolved in 2 M NaOH (0.4 mL, 4.6 equiv.), and THF (0.4 mL) was added. The mixture was stirred on ice for 10 min, and heptadecenoyl chloride dissolved in 0.2 mL of THF (49.9 mg, 0.174 mmol, 1.0 equiv.) was added drop-wise. The mixture was stirred for 1 h at ambient temperature, and then poured into ice-cold HCl. The product was extracted with EtOAc and the combined organic layers were dried over anhydrous $Na_2SO_4$ and concentrated under reduced pressure. The residue was purified by preparative TLC ($CHCl_3$:MeOH:$NH_4OH$:$H_2O$ = 65:35:5:1) providing the title compound as a white solid (25.0 mg, 40%): $^1$H NMR (600 MHz, $CDCl_3$) δ 5.36 (s, 2H), 4.34 (s, 1H), 3.99 (s, 1H), 3.76 (s, 1H), 1.21–2.37 (m, 26H), 0.91 (m, 3H). HRMS (ESI-TOF-) *m*/*z* calc'd for $C_{20}H_{36}NO_4$ $[M - H]^-$: 354.2649, found 354.2648.

## RESULTS AND DISCUSSION

### Generation and Initial Characterization of ABHD4$^{-/-}$ Mice

ABHD4$^{-/-}$ mice were generated by replacing exons three and four of the *Abhd4* gene (exon three encodes the catalytic serine) with a Neo cassette using traditional gene-targeting techniques (Figure 2A). Disruption of the genomic locus was confirmed by Southern blotting (Figure 2B and C) and PCR genotyping (Figure 2D). Loss of *Abhd4* mRNA expression and ABHD4 protein activity were confirmed by RT-PCR (Figure 2E) and activity-based protein profiling [ABPP; gel-based (Figure 2F) and mass spectrometry (MS)-based (Figure 2G and Table S1)]. ABHD4$^{-/-}$ mice were born at the expected Mendelian frequency, were viable and healthy, and showed no overt differences in their cage behavior compared to wild-type littermates. Brain homogenates from ABHD4$^{-/-}$ mice displayed significant, but incomplete reductions in NAPE- and lyso-NAPE-lipase activity compared to brain homogenates from ABHD4$^{+/+}$ mice (Figure 1H), indicating that ABHD4 is a principal, but not sole enzyme in the nervous system that hydrolyzes NAPEs and lyso-NAPEs.

### Deregulated Brain NAPE Metabolism in ABHD4$^{-/-}$ Mice

We previously showed that ABHD4 exhibits both NAPE- and lysoNAPE-lipase activity *in vitro* to sequentially produce lysoNAPEs and GP-NAEs,[17] the latter of which can be processed further to NAEs by glycerophosphodiesterase such as GDE1.[35, 43] Based on these biochemical assignments, we measured the major classes of lipids along the NAPE metabolic pathway in brain tissue from ABHD4$^{+/+}$ and ABHD4$^{-/-}$ mice. No changes in NAPE or NAE content were observed in ABHD4$^{-/-}$ brains (Figure S1). In contrast, the concentrations of multiple GP-NAEs were significantly reduced in ABHD4$^{-/-}$ brains compared to wild-type brains, with the decrease in *N*-16:0 GP-NAE being the most prominent (Figure 3A and Figure S1). The absolute concentrations of GP-NAEs were affected by the pH of the aqueous phase of the lipid extraction (see below), but, regardless,

significant reductions were observed with or without acidification of the aqueous phase (Figure 3A and Figure S1). Modest, but significant reductions in some lysoNAPEs, including *N*-16:0, *O*-18:0 and *N*-16:0, *O*-20:4 were also detected in brains from ABHD4$^{-/-}$ mice (Figure S1).

There are two primary classes of ethanolamine glycerophospholipids – diacyl-PEs and 1-alkenyl 2-acyl PEs (plasmalogens). Plasmalogen-type NAPE and lyso-NAPE (pNAPE and lyso-pNAPE, respectively) are also present in mouse brain and NAEs can be formed from these lipids through both NAPE-PLD-dependent and -independent pathways.[14] In contrast to the aforementioned minor reductions in lyso-NAPEs, the lyso-pNAPE content of ABHD4$^{-/-}$ brains was markedly decreased (Figure 3B). We found that recombinant ABHD4 expressed by transient transfection in COS-7 cells showed robust pNAPE-lipase activity (Figure 3C) and that brain lysates from ABHD4$^{-/-}$ mice exhibited significantly decreased pNAPE-lipase activity (Figure 3D). Recombinant ABHD4 displayed, on the other hand, a very limited capacity to hydrolyze plasmenyl-PE (Figure 3C) and the hydrolytic activity for this substrate was unaltered in ABHD4$^{-/-}$ brain tissue (Figure 3D). Despite substantial reductions in lyso-pNAPEs, the concentrations of pNAPEs were unaltered in brain tissue from ABHD4$^{-/-}$ mice (Figure S1).

As mentioned above, acidification of the aqueous phase during lipid extraction resulted in higher absolute concentrations of GP-NAEs and a more prominent decrease in these concentrations in ABHD4$^{-/-}$ brains that resembled the magnitude of reductions observed in brain lyso-pNAPEs. Based on the known vulnerability of alkenyl bonds to acid cleavage,[44] we speculate that acid-catalyzed breakdown of the *sn*-1 alkenyl bond of lyso-pNAPEs may contribute to accumulated GP-NAE signals under acid extraction conditions.

These data, taken together, demonstrate that ABHD4 regulates multiple, but not all components of the NAPE pathway. The substantial reductions in GP-NAEs and lyso-pNAPEs in ABHD4$^{-/-}$ brains support a physiological role for ABHD4 as a principal (lyso)-NAPE lipase in the mammalian nervous system. The more modest reductions in lyso-NAPEs could be explained by a dual role for ABHD4 in contributing to both the biosynthesis and degradation of this class of lipids (through NAPE and lyso-NAPE hydrolysis, respectively), which is not a complication for lyso-pNAPEs, since these ether lipids cannot be further hydrolyzed by ABHD4. That neither brain NAPE nor pNAPE were substantially affected by ABHD4 disruption (Figures S1C and S1D), could reflect the involvement of other metabolic pathways that control the steady-state concentrations of these lipids, such as their direct conversion to NAEs by NAPE-PLD,[13, 14] or a consequence of the much larger concentrations of (p)NAPEs compared to their downstream lyso-(p)NAPE and GP-NAE products.

## Lipidomics Identifies Deregulated NAPS Metabolism in ABHD4$^{-/-}$ Brains

We more fully characterized the metabolic changes that occur in brains from ABHD4$^{-/-}$ mice by performing untargeted MS-based lipidomic experiments. Briefly, lipid extracts were prepared using a modified Folch extraction[45] in which frozen tissue was homogenized in 2:1:1 chloroform:methanol:buffer and the lipid-containing organic layer evaporated to dryness. Lipid extracts were analyzed by LC-MS using reverse-phase chromatography and

high-resolution MS in both positive and negative modes across a mass range from 50 – 1200 *m*/*z* units. The XCMS software[42] was employed to align chromatograms across multiple independent LC-MS runs and identify substantial (> three-fold) and statistically significant ($P < 0.01$) differences in *m*/*z* value peaks between the ABHD4$^{+/+}$ and ABHD4$^{-/-}$ brain tissues. Using this approach, a major difference was observed in the negative ion mode with mass-to-charge (*m*/*z*) ratios of 380.8 and 762.5 (likely representing the $[M - 2H]^{2-}$ and $[M - H]^{-}$ ions of the same metabolite) (Figure 4A). This metabolite was substantially reduced in brains from ABHD4$^{-/-}$ mice (Figure 4A and Table S2). Several candidate structures for this metabolite were considered including phospholipids (PE and PS), lyso-NAPEs, and lyso-NAPSs, among others. Chemical synthesis of *N*-16:0/*O*-22:6 lyso-NAPE and *N*-16:0/*O*-18:0 lyso-NAPS (Figure 4B), which have the same nominal mass of 762 provided material for comparison with the endogenous *m*/*z* 762.5 metabolite. These analyses revealed that the endogenous *m*/*z* 762.5 metabolite co-eluted with *N*-16:0/*O*-18:0 lyso-NAPS (Figure 4C), whereas the retention times of the isobaric PE, lyso-NAPE, and PS species were clearly distinct (data not shown). The endogenous *m*/*z* 762.5 metabolite also gave an identical tandem MS fragmentation pattern compared to the synthetic *N*-16:0/*O*-18:0 lyso-NAPS (Figure 4D).

Taken together, these lipidomic and follow-up analytical studies indicate that ABHD4 regulates *N*-16:0/*O*-18:0 lyso-NAPS content in mouse brain.

## Deregulated Brain NAPS Metabolism in ABHD4$^{-/-}$ Mice

We next performed a broader analysis of lyso-NAPS species in ABHD4$^{+/+}$ and ABHD4$^{-/-}$ brain tissues by targeted (multiple reaction monitoring) MS. Nearly all of the *O*-16:0 and *O*-18:0 lyso-NAPS species were dramatically reduced in brain tissue from ABHD4$^{-/-}$ mice, including the most abundant detected species *N*-16:0, *O*-18:0 and *N*-16:0, *O*-18:1 (Figure 5A). In contrast, lyso-NAPS species with unsaturated *O*-fatty acyl groups on the glycerol backbone were unchanged in ABHD4$^{-/-}$ brain tissue. Conversely, modest, but significant elevations were observed in several NAPS lipids in ABHD4$^{-/-}$ brain tissue (Figure 5B). Considering that unsaturated fatty acids are generally attached at *sn*-2 position of phospholipids, these lipid profiles suggest that ABHD4 hydrolyzes the *sn*-2 fatty acyl chain of *N*-acyl phosphatidylserines (NAPSs) to produce *sn*-1-*O*-saturated lyso-NAPSs.

NAPSs are potential precursors of *N*-acyl serines (NASs), a class of bioactive lipids implicated in inflammation,[46] neuroprotection,[47, 48] and bone maintenance.[49] We did not, however, observe differences in NAS content in ABHD4$^{+/+}$ and ABHD4$^{-/-}$ brain tissues (Figure S2).

## NAPS is a Direct Substrate of ABHD4

To determine whether ABHD4 acted as an NAPS lipase, we next measured the NAPS hydrolytic activity of lysates from mock- and ABHD4-transfected COS-7 cells and found that the latter samples showed significantly elevated NAPS lipase activity when assayed either in the presence or absence of Triton-X-100 as a detergent (Figures 6A and S3). Inclusion of Triton X-100 as a detergent proportionally increased the NAPS hydrolytic activities of both mock- and ABHD4-transfected lysates (Figures 6A and S3). No

differences were detected in the PS lipase activity of mock- and ABHD4-transfected COS-7 cell lysates in the presence or absence of Triton X-100 (Figure 6A). The NAPS lipase activity of brain tissue was also substantially increased in the presence of Triton X-100, and, under these conditions, a significant reduction in NAPS (Figures 6B and S3) and (lyso)-NAPE hydrolysis (Figure S3) was detected in ABHD4$^{-/-}$ brain lysates. These data, taken together, indicate that ABHD4 serves as a general *N*-acyl phospholipid hydrolase capable of accepting both NAPEs and NAPSs as substrates. That brain tissue from ABHD4$^{-/-}$ mice still exhibits considerable *N*-acyl phospholipase activity (Figures 2H, 3D, S3, and 6B), however, points to the existence of additional lipases that may contribute to NAPE and NAPS metabolism *in vivo*.

## CONCLUSIONS

Our studies provide strong evidence that ABHD4 is a principal enzyme responsible for *N*-acyl phospholipid metabolism in the nervous system. The contribution of ABHD4 appears complementary to that of NAPE-PLD in that disruption of ABHD4 primarily affects lyso-(p)NAPE and lyso-NAPS content, while disruption of NAPE-PLD causes dramatic elevations in lyso-(p)NAPEs[13, 14]. Ablation of either enzyme alone is insufficient to produce large changes in major NAEs (e.g., C16:0, C18:0, C18:1) or anandamide, possibly indicating that these pathways can compensate for another or that additional enzymes also participate in the biosynthesis of NAEs. Future studies with NAPE-PLD$^{-/-}$/ABHD4$^{-/-}$ mice should help to address this question.

Several studies have implicated the direct involvement of NAPEs in cellular and physiological processes,[2, 3] including feeding,[8] inflammation,[9] and biomembrane stability.[6] Lyso-(p)NAPEs are less well characterized. NAPSs were only recently identified as natural brain constituents,[33, 50] and to our knowledge, lysoNAPSs have not previously been reported as endogenous metabolites in mammalian systems. Knockdown of ABHD4 has been shown to confer resistance to anoikis (or cell-detachment-induced apoptosis) in RWPE-1 prostate cells.[51] Whether this effect is mediated by *N*-acyl phospholipids, however, remains unknown. Future studies using ABHD4$^{-/-}$ mice, as well as the development of ABHD4-selective inhibitors, should strengthen our understanding of the functions of this enzyme and its *N*-acyl phospholipid substrates and products in mammalian biology and disease.

## Supplementary Material

Refer to Web version on PubMed Central for supplementary material.

## Acknowledgments

We thank K.-L. Hsu for helpful discussion and K. Masuda, H. Pugh ,T. Kambe, K. Lum and D. Ogasawara for technical assistance.

**Funding**

This work was supported by the National Institutes of Health grant R01 DA033760 (B.F.C.) and a Japanese Society for the Promotion of Science Scholarship (H.L.).

## REFERENCES


1. Muro E, Atilla-Gokcumen GE, Eggert US. Lipids in cell biology: how can we understand them better? Molecular biology of the cell. 2014; 25:1819–1823. [PubMed: 24925915]
2. Wellner N, Diep TA, Janfelt C, Hansen HS. N-acylation of phosphatidylethanolamine and its biological functions in mammals. Biochimica et biophysica acta. 2013; 1831:652–662. [PubMed: 23000428]
3. Coulon D, Faure L, Salmon M, Wattelet V, Bessoule JJ. Occurrence, biosynthesis and functions of N-acylphosphatidylethanolamines (NAPE): not just precursors of N-acylethanolamines (NAE). Biochimie. 2012; 94:75–85. [PubMed: 21575672]
4. Matsumoto M, Miwa M. Study on the new phospholipid, N-acyl-I-alkyl glycerophosphorylethanolamine, from bovine erythrocytes. Biochimica et biophysica acta. 1973; 296:350–364. [PubMed: 4688439]
5. Epps DE, Natarajan V, Schmid PC, Schmid HO. Accumulation of N-acylethanolamine glycerophospholipids in infarcted myocardium. Biochimica et biophysica acta. 1980; 618:420–430. [PubMed: 7397206]
6. Sandoval JA, Huang ZH, Garrett DC, Gage DA, Chapman KD. N-acylphosphatidylethanolamine in dry and imbibing cottonseeds. Amounts, molecular species, and enzymatic synthesis. Plant physiology. 1995; 109:269–275. [PubMed: 7480326]
7. Shangguan T, Pak CC, Ali S, Janoff AS, Meers P. Cation-dependent fusogenicity of an N-acyl phosphatidylethanolamine. Biochimica et biophysica acta. 1998; 1368:171–183. [PubMed: 9459596]
8. Gillum MP, Zhang D, Zhang XM, Erion DM, Jamison RA, Choi C, Dong J, Shanabrough M, Duenas HR, Frederick DW, Hsiao JJ, Horvath TL, Lo CM, Tso P, Cline GW, Shulman GI. N-acylphosphatidylethanolamine, a gut-derived circulating factor induced by fat ingestion, inhibits food intake. Cell. 2008; 135:813–824. [PubMed: 19041747]
9. Shiratsuchi A, Ichiki M, Okamoto Y, Ueda N, Sugimoto N, Takuwa Y, Nakanishi Y. Inhibitory effect of N-palmitoylphosphatidylethanolamine on macrophage phagocytosis through inhibition of Rac1 and Cdc42. Journal of biochemistry. 2009; 145:43–50. [PubMed: 18974159]
10. Ueda N, Tsuboi K, Uyama T. Enzymological studies on the biosynthesis of N-acylethanolamines. Biochimica et biophysica acta. 2010; 1801:1274–1285. [PubMed: 20736084]
11. Schmid PC, Reddy PV, Natarajan V, Schmid HH. Metabolism of N-acylethanolamine phospholipids by a mammalian phosphodiesterase of the phospholipase D type. The Journal of biological chemistry. 1983; 258:9302–9306. [PubMed: 6308001]
12. Okamoto Y, Morishita J, Tsuboi K, Tonai T, Ueda N. Molecular characterization of a phospholipase D generating anandamide and its congeners. The Journal of biological chemistry. 2004; 279:5298–5305. [PubMed: 14634025]
13. Leung D, Saghatelian A, Simon GM, Cravatt BF. Inactivation of N-acyl phosphatidylethanolamine phospholipase D reveals multiple mechanisms for the biosynthesis of endocannabinoids. Biochemistry. 2006; 45:4720–4726. [PubMed: 16605240]
14. Tsuboi K, Okamoto Y, Ikematsu N, Inoue M, Shimizu Y, Uyama T, Wang J, Deutsch DG, Burns MP, Ulloa NM, Tokumura A, Ueda N. Enzymatic formation of N-acylethanolamines from N-acylethanolamine plasmalogen through N-acylphosphatidylethanolamine-hydrolyzing phospholipase D-dependent and -independent pathways. Biochimica et biophysica acta. 2011; 1811:565–577. [PubMed: 21801852]
15. Natarajan V, Schmid PC, Reddy PV, Schmid HH. Catabolism of N-acylethanolamine phospholipids by dog brain preparations. Journal of neurochemistry. 1984; 42:1613–1619. [PubMed: 6726229]
16. Sun YX, Tsuboi K, Okamoto Y, Tonai T, Murakami M, Kudo I, Ueda N. Biosynthesis of anandamide and N-palmitoylethanolamine by sequential actions of phospholipase A2 and lysophospholipase D. The Biochemical journal. 2004; 380:749–756. [PubMed: 14998370]
17. Simon GM, Cravatt BF. Endocannabinoid biosynthesis proceeding through glycerophospho-N-acyl ethanolamine and a role for alpha/beta-hydrolase 4 in this pathway. The Journal of biological chemistry. 2006; 281:26465–26472. [PubMed: 16818490]

18. Liu J, Wang L, Harvey-White J, Osei-Hyiaman D, Razdan R, Gong Q, Chan AC, Zhou Z, Huang BX, Kim HY, Kunos G. A biosynthetic pathway for anandamide. Proceedings of the National Academy of Sciences of the United States of America. 2006; 103:13345–13350. [PubMed: 16938887]
19. Liu J, Wang L, Harvey-White J, Huang BX, Kim HY, Luquet S, Palmiter RD, Krystal G, Rai R, Mahadevan A, Razdan RK, Kunos G. Multiple pathways involved in the biosynthesis of anandamide. Neuropharmacology. 2008; 54:1–7. [PubMed: 17631919]
20. Natarajan V, Reddy PV, Schmid PC, Schmid HH. N-Acylation of ethanolamine phospholipids in canine myocardium. Biochimica et biophysica acta. 1982; 712:342–355. [PubMed: 7126608]
21. Cadas H, Gaillet S, Beltramo M, Venance L, Piomelli D. Biosynthesis of an endogenous cannabinoid precursor in neurons and its control by calcium and cAMP. The Journal of neuroscience : the official journal of the Society for Neuroscience. 1996; 16:3934–3942. [PubMed: 8656287]
22. Reddy PV, Natarajan V, Schmid PC, Schmid HH. N-Acylation of dog heart ethanolamine phospholipids by transacylase activity. Biochimica et biophysica acta. 1983; 750:472–480. [PubMed: 6824721]
23. Cadas H, di Tomaso E, Piomelli D. Occurrence and biosynthesis of endogenous cannabinoid precursor, N-arachidonoyl phosphatidylethanolamine, in rat brain. The Journal of neuroscience : the official journal of the Society for Neuroscience. 1997; 17:1226–1242. [PubMed: 9006968]
24. Schmid HH. Pathways and mechanisms of N-acylethanolamine biosynthesis: can anandamide be generated selectively? Chemistry and physics of lipids. 2000; 108:71–87. [PubMed: 11106783]
25. Jin XH, Okamoto Y, Morishita J, Tsuboi K, Tonai T, Ueda N. Discovery and characterization of a Ca2+-independent phosphatidylethanolamine N-acyltransferase generating the anandamide precursor and its congeners. The Journal of biological chemistry. 2007; 282:3614–3623. [PubMed: 17158102]
26. Shinohara N, Uyama T, Jin XH, Tsuboi K, Tonai T, Houchi H, Ueda N. Enzymological analysis of the tumor suppressor A-C1 reveals a novel group of phospholipid-metabolizing enzymes. Journal of lipid research. 2011; 52:1927–1935. [PubMed: 21880860]
27. Jin XH, Uyama T, Wang J, Okamoto Y, Tonai T, Ueda N. cDNA cloning and characterization of human and mouse Ca(2+)-independent phosphatidylethanolamine N-acyltransferases. Biochimica et biophysica acta. 2009; 1791:32–38. [PubMed: 19000777]
28. Uyama T, Morishita J, Jin XH, Okamoto Y, Tsuboi K, Ueda N. The tumor suppressor gene H-Rev107 functions as a novel Ca2+-independent cytosolic phospholipase A1/2 of the thiol hydrolase type. Journal of lipid research. 2009; 50:685–693. [PubMed: 19047760]
29. Uyama T, Jin XH, Tsuboi K, Tonai T, Ueda N. Characterization of the human tumor suppressors TIG3 and HRASLS2 as phospholipid-metabolizing enzymes. Biochimica et biophysica acta. 2009; 1791:1114–1124. [PubMed: 19615464]
30. Uyama T, Inoue M, Okamoto Y, Shinohara N, Tai T, Tsuboi K, Inoue T, Tokumura A, Ueda N. Involvement of phospholipase A/acyltransferase-1 in N-acylphosphatidylethanolamine generation. Biochimica et biophysica acta. 2013; 1831:1690–1701. [PubMed: 23994608]
31. Uyama T, Ikematsu N, Inoue M, Shinohara N, Jin XH, Tsuboi K, Tonai T, Tokumura A, Ueda N. Generation of N-acylphosphatidylethanolamine by members of the phospholipase A/acyltransferase (PLA/AT) family. The Journal of biological chemistry. 2012; 287:31905–31919. [PubMed: 22825852]
32. Golczak M, Kiser PD, Sears AE, Lodowski DT, Blaner WS, Palczewski K. Structural basis for the acyltransferase activity of lecithin:retinol acyltransferase-like proteins. The Journal of biological chemistry. 2012; 287:23790–23807. [PubMed: 22605381]
33. Guan Z, Li S, Smith DC, Shaw WA, Raetz CR. Identification of N-acylphosphatidylserine molecules in eukaryotic cells. Biochemistry. 2007; 46:14500–14513. [PubMed: 18031065]
34. Wood PL. Accumulation of N-Acylphosphatidylserines and N-Acylserines in the Frontal Cortex in Schizophrenia. Neurotransmitter. 2014; 1
35. Simon GM, Cravatt BF. Anandamide biosynthesis catalyzed by the phosphodiesterase GDE1 and detection of glycerophospho-N-acyl ethanolamine precursors in mouse brain. The Journal of biological chemistry. 2008; 283:9341–9349. [PubMed: 18227059]

36. Bartlett GR. Phosphorus assay in column chromatography. The Journal of biological chemistry. 1959; 234:466–468. [PubMed: 13641241]
37. Kamat SS, Camara K. Immunomodulatory lysophosphatidylserines are regulated by ABHD16A and ABHD12 interplay. 2015; 11:164–171.
38. Jessani N, Niessen S, Wei BQ, Nicolau M, Humphrey M, Ji Y, Han W, Noh DY, Yates JR 3rd, Jeffrey SS, Cravatt BF. A streamlined platform for high-content functional proteomics of primary human specimens. Nature methods. 2005; 2:691–697. [PubMed: 16118640]
39. Bligh EG, Dyer WJ. A rapid method of total lipid extraction and purification. Canadian journal of biochemistry and physiology. 1959; 37:911–917. [PubMed: 13671378]
40. Saghatelian A, Trauger SA, Want EJ, Hawkins EG, Siuzdak G, Cravatt BF. Assignment of endogenous substrates to enzymes by global metabolite profiling. Biochemistry. 2004; 43:14332–14339. [PubMed: 15533037]
41. Tautenhahn R, Patti GJ, Rinehart D, Siuzdak G. XCMS Online: a web-based platform to process untargeted metabolomic data. Analytical chemistry. 2012; 84:5035–5039. [PubMed: 22533540]
42. Smith CA, Want EJ, O'Maille G, Abagyan R, Siuzdak G. XCMS: processing mass spectrometry data for metabolite profiling using nonlinear peak alignment, matching, and identification. Analytical chemistry. 2006; 78:779–787. [PubMed: 16448051]
43. Simon GM, Cravatt BF. Characterization of mice lacking candidate N-acyl ethanolamine biosynthetic enzymes provides evidence for multiple pathways that contribute to endocannabinoid production in vivo. Molecular bioSystems. 2010; 6:1411–1418. [PubMed: 20393650]
44. Dawson RM. A hydrolytic procedure for the identification and estimation of individual phospholipids in biological samples. The Biochemical journal. 1960; 75:45–53. [PubMed: 13814585]
45. Folch J, Lees M, Sloane Stanley GH. A simple method for the isolation and purification of total lipides from animal tissues. The Journal of biological chemistry. 1957; 226:497–509. [PubMed: 13428781]
46. Milman G, Maor Y, Abu-Lafi S, Horowitz M, Gallily R, Batkai S, Mo FM, Offertaler L, Pacher P, Kunos G, Mechoulam R. N-arachidonoyl L-serine, an endocannabinoid-like brain constituent with vasodilatory properties. Proceedings of the National Academy of Sciences of the United States of America. 2006; 103:2428–2433. [PubMed: 16467152]
47. Cohen-Yeshurun A, Willner D, Trembovler V, Alexandrovich A, Mechoulam R, Shohami E, Leker RR. N-arachidonoyl-L-serine (AraS) possesses proneurogenic properties in vitro and in vivo after traumatic brain injury. Journal of cerebral blood flow and metabolism : official journal of the International Society of Cerebral Blood Flow and Metabolism. 2013; 33:1242–1250.
48. Cohen-Yeshurun A, Trembovler V, Alexandrovich A, Ryberg E, Greasley PJ, Mechoulam R, Shohami E, Leker RR. N-arachidonoyl-L-serine is neuroprotective after traumatic brain injury by reducing apoptosis. Journal of cerebral blood flow and metabolism : official journal of the International Society of Cerebral Blood Flow and Metabolism. 2011; 31:1768–1777.
49. Smoum R, Bar A, Tan B, Milman G, Attar-Namdar M, Ofek O, Stuart JM, Bajayo A, Tam J, Kram V, O'Dell D, Walker MJ, Bradshaw HB, Bab I, Mechoulam R. Oleoyl serine, an endogenous N-acyl amide, modulates bone remodeling and mass. Proceedings of the National Academy of Sciences of the United States of America. 2010; 107:17710–17715. [PubMed: 20876113]
50. Guan Z. Discovering novel brain lipids by liquid chromatography/tandem mass spectrometry. Journal of chromatography. B, Analytical technologies in the biomedical and life sciences. 2009; 877:2814–2821. [PubMed: 19303823]
51. Simpson CD, Hurren R, Kasimer D, MacLean N, Eberhard Y, Ketela T, Moffat J, Schimmer AD. A genome wide shRNA screen identifies alpha/beta hydrolase domain containing 4 (ABHD4) as a novel regulator of anoikis resistance. Apoptosis : an international journal on programmed cell death. 2012; 17:666–678. [PubMed: 22488300]

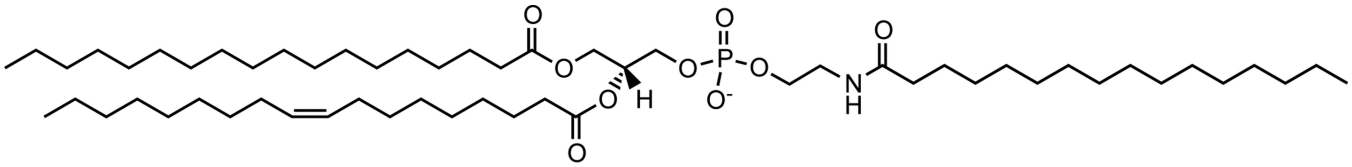

*N*-16:0 *sn*-1-*O*-18:0 *sn*-2-*O*-18:1 NAPE

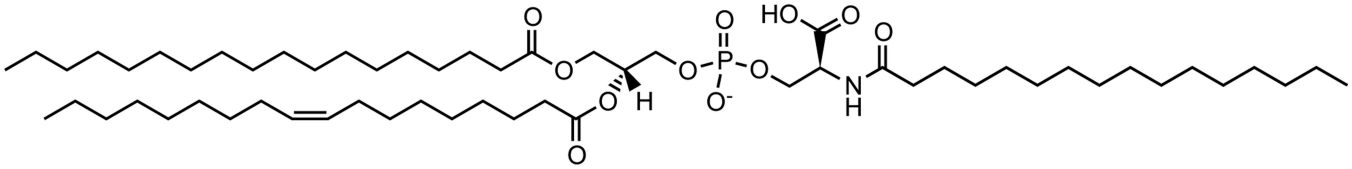

*N*-16:0 *sn*-1-*O*-18:0 *sn*-2-*O*-18:1 NAPS

**Figure 1. *N*-acyl Phospholipids**

Structures of representative *N*-acyl phosphatidylethanolamine (NAPE) and *N*-acyl phosphatidylserine (NAPS) lipids.

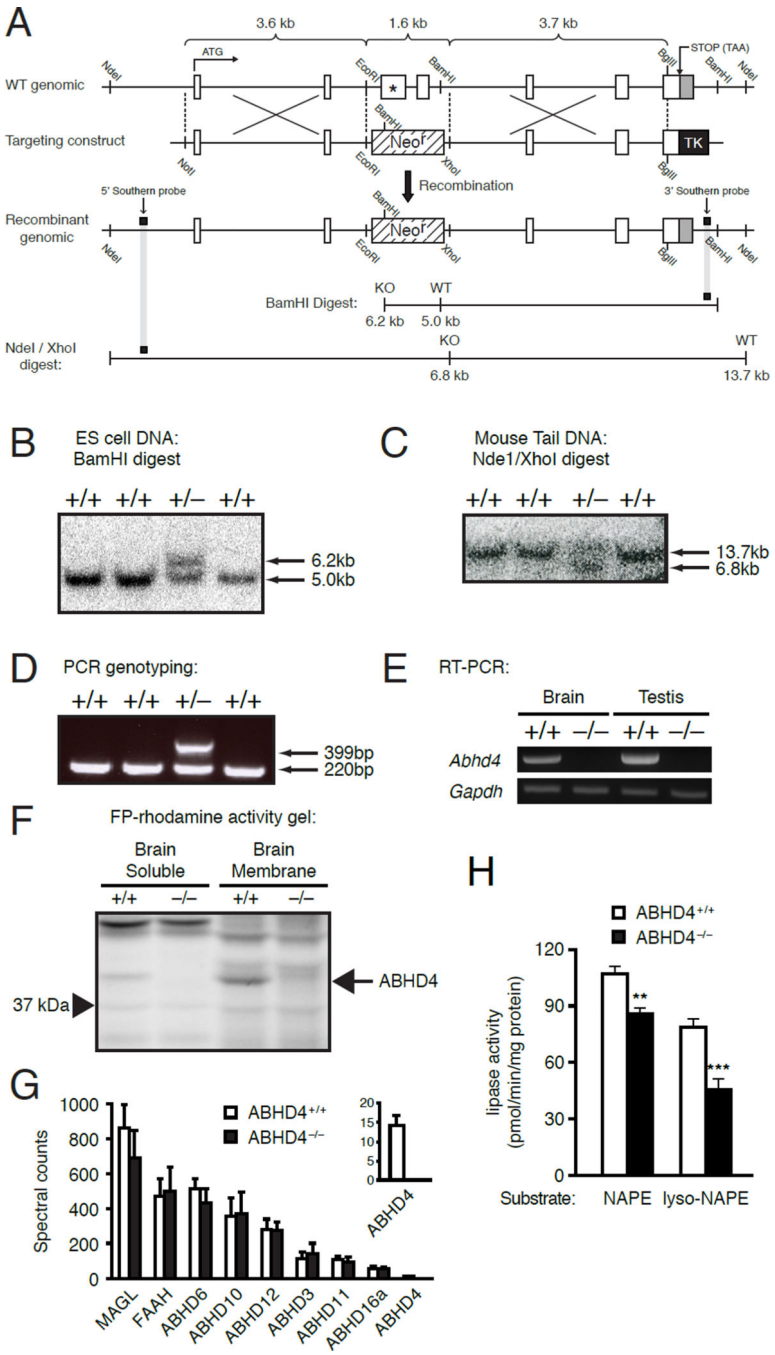


**Figure 2. Generation and initial characterization of ABHD4$^{-/-}$ mice**

(A) The genomic structure of the *Abhd4* genomic locus on chromosome 14 is shown, along with the targeting construct with regions of homology flanking exons 3 and 4 (which contains the catalytic serine; asterisk) and the final recombined locus. Only relevant restriction sites are designated. The positions of probes for Southern hybridization and the gene fragments expected upon Southern blotting with the indicated probes and restriction enzymes are also shown.

(B) Southern blot of BamHI-digested ES cell DNA showing a clone with targeted disruption of the *Abhd4* gene.
(C) Southern blot of NdeI/XhoI-digested tail-DNA from ABHD4$^{+/+}$ and ABHD4$^{+/-}$ mice demonstrating germ-line transmission.
(D) PCR genotyping in which the ABHD4$^{+/+}$ locus is identified by a 220 bp band and the ABHD4$^{-/-}$ locus is identified by a 399 bp band.
(E) RT-PCR analysis confirmed loss of *Abhd4* mRNA expression in brain and testis tissues from ABHD4$^{-/-}$ mice.
(F) ABPP of soluble and membrane fractions of brain tissue from ABHD4$^{+/+}$ and ABHD4$^{-/-}$ mice using the serine hydrolase-directed probe FP-rhodamine shows that active ABHD4 protein is not observed in ABHD4$^{-/-}$ mice.
(G) Lack of ABHD4 activity in ABHD4$^{-/-}$ brains was confirmed by the MS-based proteomic method ABPP-MudPIT using the probe FP-biotin. The activity of representative serine hydrolases is shown. See Table S1 for a complete list of detected serine hydrolases.
(H) Soluble fractions of brain tissue from ABHD4$^{+/+}$ and ABHD4$^{-/-}$ mice were incubated with NAPE (1,2-dioleoyl-*sn*-glycero-3-phospho (*N*-arachidonoyl) ethanolamine) or lyso-NAPE (1-oleoyl-2-hydroxy-*sn*-glycero-3-phospho (*N*-palmitoyl) ethanolamine) and hydrolytic activity was quantified by measuring lyso-NAPE and oleic acid release, respectively. Data represent mean values ± SEM ($n$ = 5). **, $P < 0.01$; ***, $P < 0.001$. Unpaired, two-tailed t test was used.

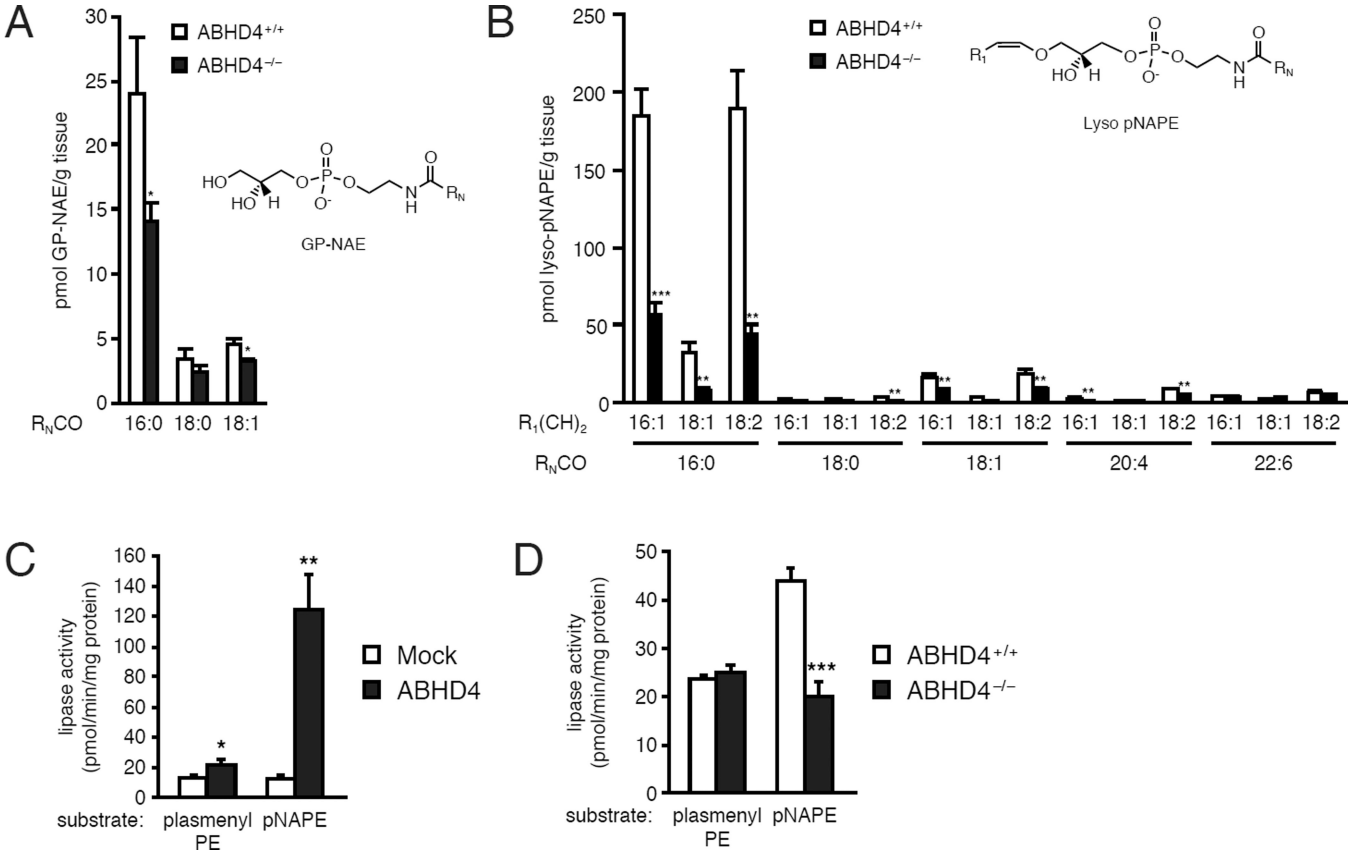


**Figure 3. GP-NAEs and lyso-pNAPEs are decreased in brain tissue from ABHD4$^{-/-}$ mice**

(A–B) Targeted mass-spectrometry-based estimates of GP-NAE (A) and lyso-pNAPE (B) abundance in brain tissue from ABHD4$^{+/+}$ and ABHD4$^{-/-}$ mice. Data represent mean values ± SEM ($n$ = 8 for A, $n$ = 5 for B). *, $P < 0.05$; **, $P < 0.01$; ***, $P < 0.001$. Unpaired, two-tailed t test was used.

(C, D) Soluble fractions of mock- and ABHD4-transfected COS-7 cell extracts (C) or brain tissue from ABHD4$^{+/+}$ and ABHD4$^{-/-}$ mice (D) were incubated with plasmenyl PE (1-*O*-1'-(*Z*)-octadecenyl-2-oleoyl-*sn*-glycero-3-phosphoethanolamine) or pNAPE (1-*O*-1'-(*Z*)-octadecenyl-2-oleoyl-*sn*-glycero-3-phospho (*N*-palmitoyl) ethanolamine), and hydrolytic activity was quantified by measuring oleic acid release. Data represent mean values ± SEM ($n$ = 4). *, $P < 0.05$; **, $P < 0.01$; ***, $P < 0.001$. Unpaired, two-tailed t test was used. See also Figure S1.

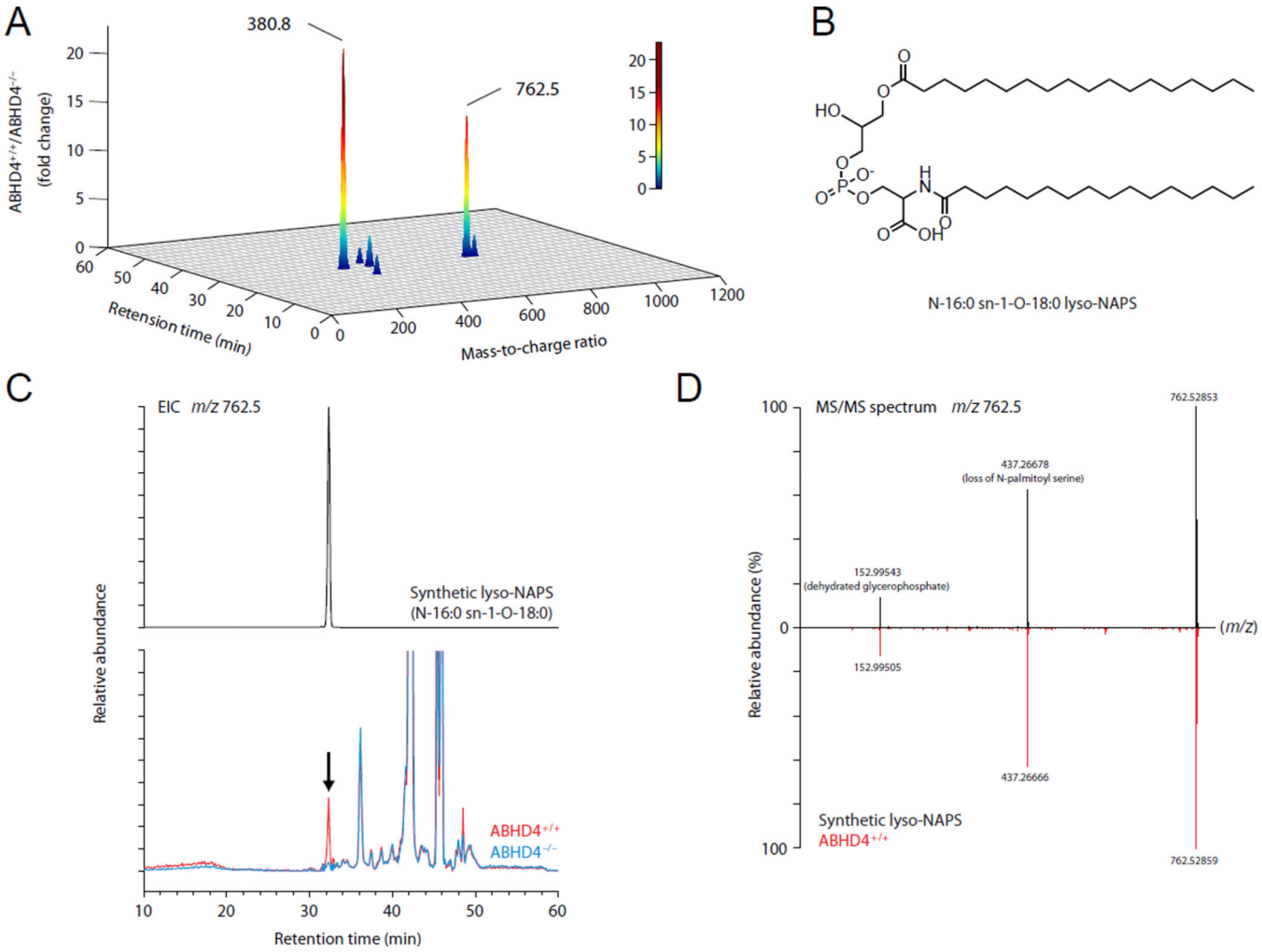


**Figure 4. Lipidomic analysis of ABHD4$^{-/-}$ mice brains**

(A) Changes in brain metabolites in ABHD4$^{+/+}$ versus ABHD4$^{-/-}$ brains were measured by untargeted LC-MS. A metabolite with *m*/*z* 380.8 and 762.5 was profoundly decreased in brains from ABHD4$^{-/-}$ mice compared with ABHD4$^{+/+}$ mice. (B) Structure of *N*-16:0/*sn*-1-*O*-18:0 lyso-NAPS (1-stearoyl-2-oleoyl-*sn*-glycero-3-phospho (*N*-palmitoyl) serine). (C, D) The *m*/*z* 762.5 metabolite (red trace) in brain tissue from ABHD4$^{+/+}$ mice exhibited the same LC elution time (C) and MS/MS fragmentation pattern (D) as a synthetic *N*-16:0 *O*-18:0 lyso-NAPS standard (black trace). The decrease of the *m*/*z* 762.5 metabolite in ABHD4$^{-/-}$ mice is also evident (blue trace). Key daughter ions in the MS/MS analysis include 153.0 (dehydrated glycerophosphate) and 437.3 [loss of *N*-palmitoyl serine (*O*-18:0 lysophosphatidic acid)].

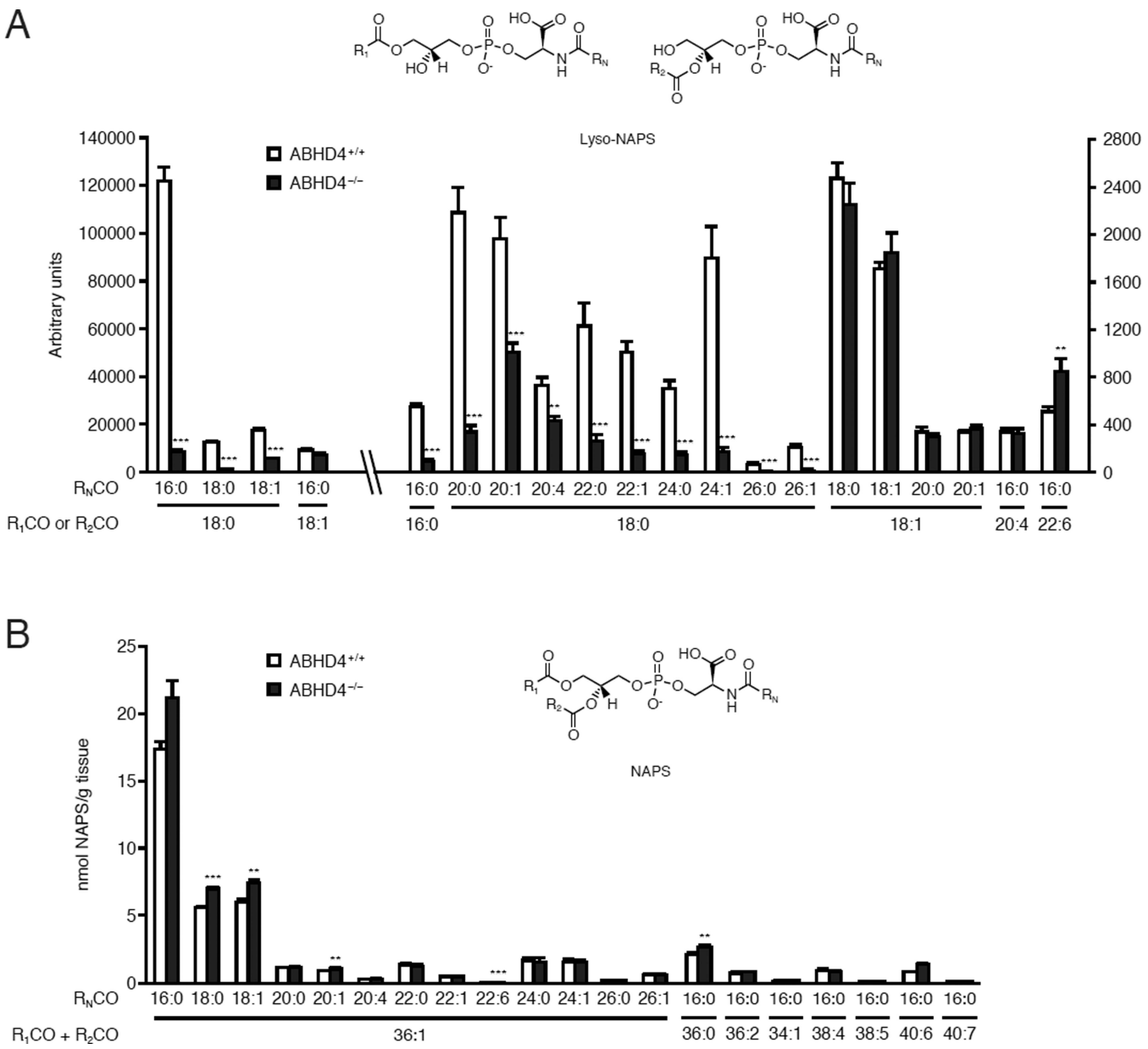


**Figure 5. Lyso-NAPSs are decreased in brain tissue from ABHD4$^{-/-}$ mice**

Targeted MS-based estimates of lyso-NAPS (A) and NAPS (B) abundance in brain tissue from ABHD4$^{+/+}$ and ABHD4$^{-/-}$ mice. Lyso-NAPS measurements are reported in arbitrary units. Data represent mean values ± SEM ($n$ = 8 for A, $n$ = 5 for B). **, $P < 0.01$; ***, $P < 0.001$. Unpaired, two-tailed t test was used.

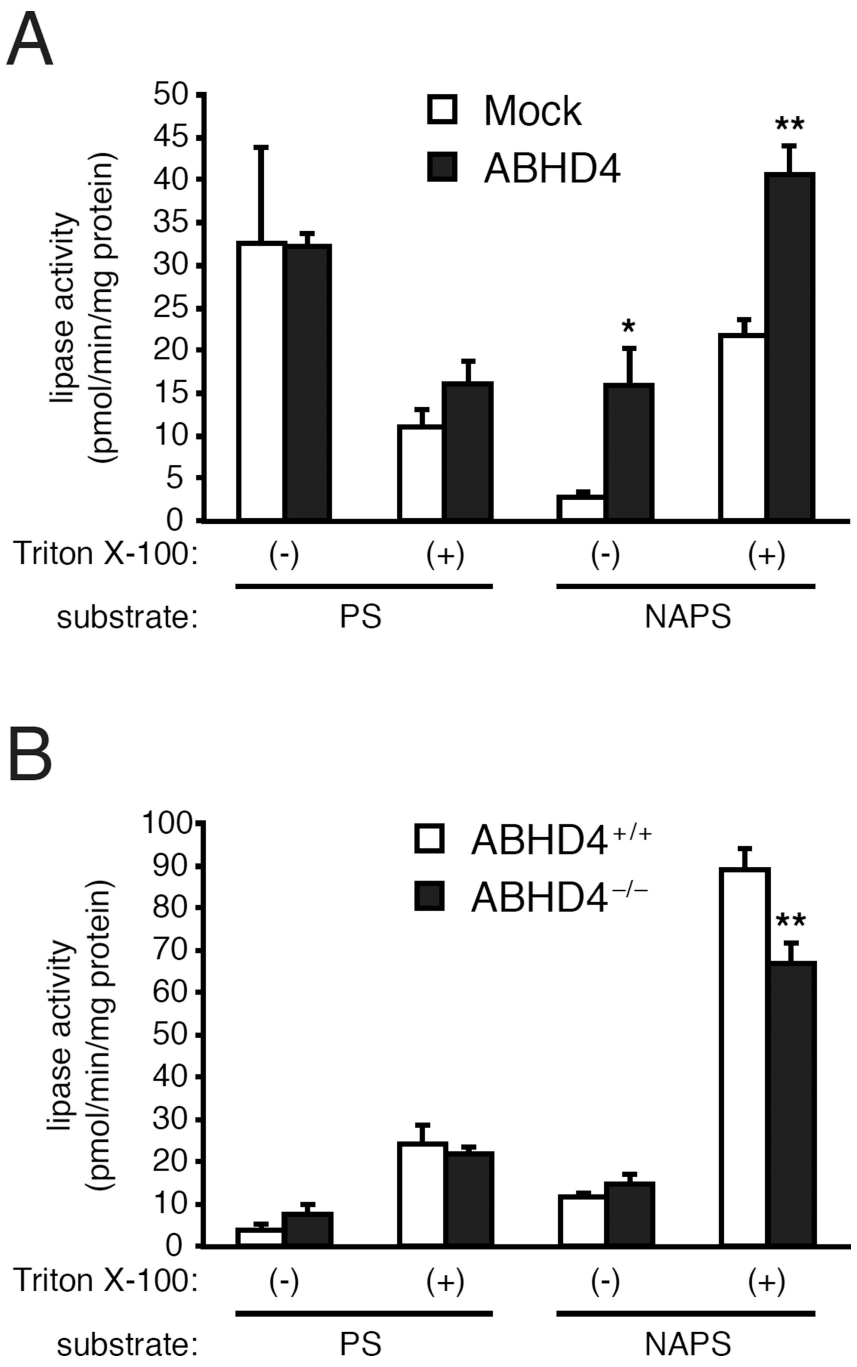


**Figure 6. ABHD4 exhibits NAPS-lipase activity**

Soluble fractions of mock- and ABHD4-transfected COS-7 cell extracts (A) or brain tissue from ABHD4$^{+/+}$ and ABHD4$^{-/-}$ mice (B) were incubated with PS (1-stearoyl-2-oleoyl-*sn*-glycero-3-phosphoserine) or NAPS (1-stearoyl-2-oleoyl-*sn*-glycero-3-phospho (*N*-palmitoyl) serine) and hydrolytic activity was quantified by measuring oleic acid release in the absence or presence of 0.1% of Triton X-100. Also see Figure S3 for measurement of NAPS hydrolysis by quantifying release of lyso-NAPS product. Data represent mean values

± SEM ($n$ = 4 for A, $n$ = 5 for B). *, $P < 0.05$; **, $P < 0.01$. Unpaired, two-tailed t test was used.